Letter

Coverage-Dependent Site-Specific Placement and Correlated Diffusion of Atomic Oxygen on Moiré-Patterned Graphene on Ru(0001)
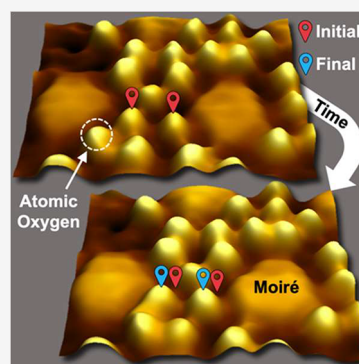
Joshua Wagner and Steven J. Sibener*

Read Online

ACCESS | 📊 Metrics & More | 📄 Article Recommendations

ABSTRACT: Nano-periodic arrays of atomic oxygen are visualized on epitaxial graphene on Ru(0001) *via* STM following supersonic beam exposure to non-equilibrium fluxes of atomic oxygen. Self-organization of atomic oxygen on graphene is directed by the intrinsic moiré pattern of the ruthenium−graphene interface. Atom-resolved STM imaging reveals the richness of multiparticle interactions, leading to correlated atomic diffusion and placement. Pair-distribution functions demonstrate that repulsive oxygen−oxygen interactions play an increasingly important role in the site specificity and diffusivity of atomic oxygen on the moiré lattice with increasing coverage. Atomic visualization shows the number of oxygen atoms in a local region changes overall diffusion rates and promotes the correlated motion of oxygen atoms. Understanding the site specificity of oxygen adsorption and diffusive behavior of atomic oxygen on epitaxial graphene on Ru(0001) provides insight for both the synthesis and stability of moiré-templated two-dimensional materials which show promise as platforms for next-generation quantum materials and catalysts.

Two-dimensional (2D) materials are next-generation platforms for quantum devices, efficient catalysts, and applications in photonics, electronics, and sensing.[1−4] In the effort to develop such platforms, the intentional moiré patterning of 2D materials promises impressive tunability of physical properties and spatial patterning through choice of material and degree of rotation.[5,6] Further interest comes from the oxidation mechanisms of graphitic materials in aggressive chemical environments.[7] At the intersection of the fields of 2D materials, controlled materials oxidation, and quantum science is the moiré-templated oxidation of graphene on ruthenium.

Directed placement of atomic oxygen is achieved herein through preferential surface binding at specific moiré lattice sites, and results illustrate the formation of nano-periodic self-assembled arrays of adsorbed atomic oxygen. The site specificity of adatom binding is found to be influenced by the coverage of atomic oxygen, and oxygen−oxygen interactions influence both the placement and the diffusivity of oxygen. Results have implications for the creation and stability of moiré-directed self-assembled 2D materials.

Oxidation of epitaxial graphene (G/Ru(0001)) is directed by the 3 nm hexagonal periodicity of the G/Ru(0001) moiré pattern. The chemical stability of surface structures is greatly influenced by the atomic stacking of graphene and ruthenium lattice cells with three distinct regions—FCC, HCP, and atop—readily distinguishable *via* STM.[8−11] Crystallographic examination at the Swiss Light Source determined the moiré pattern of G/Ru(0001) to be the result of a massive 25 × 25

supercell of graphene laid over 23 × 23 Ru atoms and showed bonding between Ru(0001) and graphene that cannot be explained by van der Waals forces alone.[12] The HCP and FCC regions experience strong hybridization with the Ru(0001) surface as these are regions in which carbon atoms sit directly atop ruthenium atoms maximizing π−d hybridization, and DFT calculations show that the hollow site carbon atoms (Figure 1a), where atomic oxygen binds, bind more strongly to the ruthenium surface in FCC than in HCP regions.[13,14] Meanwhile, the atop region has an electronic structure like that of free-standing graphene.[8,14] This difference in electronic character between HCP/FCC and atop regions provides differential reactivity and therefore directs the adsorption of atomic oxygen. Variability in surface dynamics and binding as a function of substrate provides additional tunability for the modification of 2D materials.[13,15−17]

Building on recent developments in forming self-organized nanoscale arrays of atoms/molecules on moiré materials,[18−21] we report that moiré templating can provide an avenue for the creation of large-scale homogeneously functionalized oxidized graphene surfaces using O(^{3}P) impinging on G/Ru(0001) as a
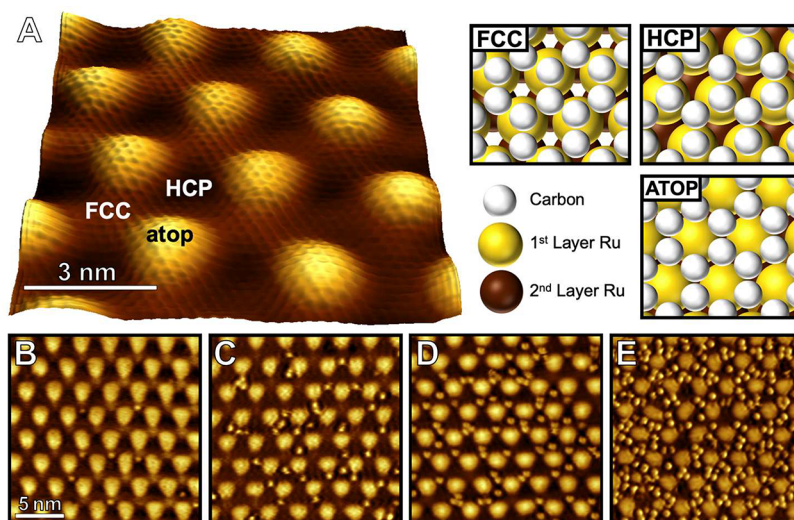
Figure 1. G/Ru(0001) before and after exposure to O(^{3}P) exposure. (A) STM image of G/Ru(0001) with its characteristic 3 nm periodic moiré pattern (10 mV, 2.3 nA, 298 K). Individual graphene unit cells are visible in the STM topography. Regions of interest in the moiré pattern are labeled, and their atomic packings are sketched on the right. (B–E) STM images (−1.5 V, −250 pA, 298 K) of G/Ru(0001) show the surface coverage of atomic oxygen increasing with progressively higher doses of O(^{3}P) impinging normal with an average kinetic energy of 0.07 eV to the surface. Exposures of 0.41 (B), 1.0 (C), 4.1 (D), and 8.2 O/nm^2 (E) are shown.

model system. Given that atomic oxygen has been shown to provide nucleation sites for metal oxide nanoparticle growth on graphene's otherwise inert basal plane,[4] moiré-templated oxidation of graphene is an auspicious launching point for the atom-by-atom synthesis of rationally designed well-ordered quantum materials.

Beyond the materials chemistry implications of moiré-templated oxidation of graphene, the reaction dynamics of atomic oxygen with graphene are nontrivial.[22] The reactivity of ground-state atomic oxygen O(^{3}P) with free-standing graphene is a spin-forbidden process resulting in a low sticking probability (∼10%) at room temperature for what should be a nearly barrierless reaction.[23] Emphasizing the effects of intersystem crossing, O(^{1}D) reactive scattering on graphene has a sticking coefficient nearly an order of magnitude higher.[23] Visualization of the products of reactive scattering of kinetic energy controlled O(^{3}P) on moiré-patterned epitaxial graphene opens a new regime of surface dynamics on a highly corrugated potential energy surfaces probed only through the introduction of kinks, steps, vacancies, and heteroatoms on single crystalline model surfaces.[24,25]

Herein, we explore the moiré-templated reactive scattering of atomic oxygen on G/Ru(0001) using an *in situ* STM in line with a molecular beam to provide *atomic visualization* of material modification after exposure to O(^{3}P). Adsorbate interactions, site specificity of binding, and surface diffusion are evaluated at increasing oxygen coverages, and results illustrate the moiré-templated introduction of atomic oxygen on 2D materials, which may serve as a platform for next-generation quantum devices.

A representative STM image of a pristine G/Ru(0001) surface is shown in Figure 1A in which individual graphene unit cells are visible. Three separate areas on the moiré pattern are discernible: FCC, HCP, and atop regions referring to the stacking of Ru atoms and graphene unit cells. These areas are sketched in Figure 1A.

Upon exposure to O(^{3}P), O atoms can be seen to occupy the HCP and FCC areas of the moiré lattice. STM imaging

(−1.5 V, −250 pA) visualizes these oxygen species as protrusions approximately 1 Å high and 5 Å wide (Figure 1B–E). Results fit well with the previous observation that oxygen atoms preferentially bind at FCC over HCP sites in the low coverage limit and have an energy difference of ∼0.05 eV between binding sites and diffusion barriers of 1.2 and 0.9 eV, respectively;[13] however, significant barriers to diffusion and molecular beam exposures of O(^{3}P) enable the visualization of non-equilibrium distributions of oxygen species on the surface with increasing coverage. The populations of O atoms adsorbing in the two regions can be predicted using a dual-site Langmuir adsorption model:[26]

$$\frac{N_{\text{HCP}}}{N_{\text{FCC}}} = \frac{\Gamma_{\text{HCP}}V_{\text{HCP}}}{\Gamma_{\text{FCC}}V_{\text{FCC}}}e^{\Delta E/k_{\text{B}}T} = e^{\Delta E/k_{\text{B}}T} \tag{1}$$

Due to symmetry in the moiré lattice, the product of surface sites (Γ) and their volume (V) is equivalent for HCP and FCC sites—leaving only the exponential term in eq 1 with $k_{\text{B}}T$ representing the hyperthermal beam energy and ΔE representing the difference in adsorption energy for atomic oxygen in HCP vs FCC sites. Immediately after O(^{3}P) exposure, O atoms exist in the HCP and FCC regions in an approximate 1:3 ratio on a 300 K G/Ru(0001) surface. These populations and an average incident atomic oxygen energy of 0.07 eV show the adsorption energy in FCC sites to be 0.08 ± 0.04 eV more stable than in HCP regions using eq 1. Uncertainty in this measurement is calculated from the FWHM of the kinetic energy of O atoms in the molecular beam. Previous results from experimental (0.05 eV)[13] and DFT calculations (0.12 eV)[13] of HCP/FCC binding in the low coverage limit fit within our hyperthermal result. Net migration from hyperthermally populated HCP sites to more stable FCC regions is limited by high barriers to diffusion. Oxygen atoms approach thermalized surface populations (HCP:FCC ≈ 1:6) on the time scale of days due to low diffusion rates at 300 K.

As the oxygen coverage increases, the HCP:FCC ratio approaches 1:1. Parity in binding between HCP and FCC sites is approached far below saturation coverages, e.g., at an average
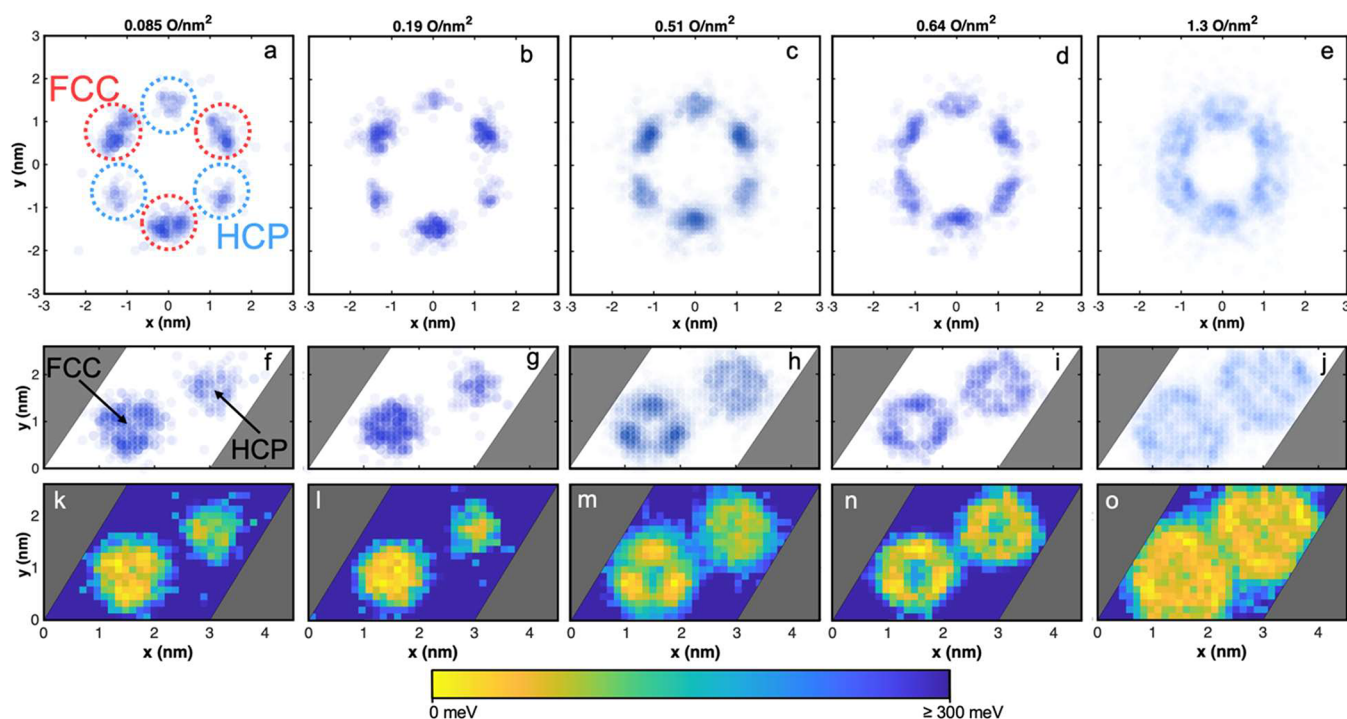
Figure 2. Site specificity and energetics of binding of oxygen on G/Ru(0001). (a−e) The location of each oxygen atom is plotted in relation to the center of the nearest moiré atop region with increasing coverage 0.085−1.3 O/nm^2. (f−j) The location of every oxygen atom is plotted on a moiré unit cell. A coverage of 1.3 O/nm^2 corresponds to 10 oxygen atoms per 12 × 11 graphene unit cell. Color has been normalized in (a−j) to show probability of finding an O atom at a particular moiré region for a given oxygen coverage. (k−o) Populations of O atoms from (f−j) are used to calculate effective adsorption energies for each oxygen coverage. The color scale in (k−o) shows adsorption energies across the moiré unit cell in comparison to the most stable binding area at that coverage.
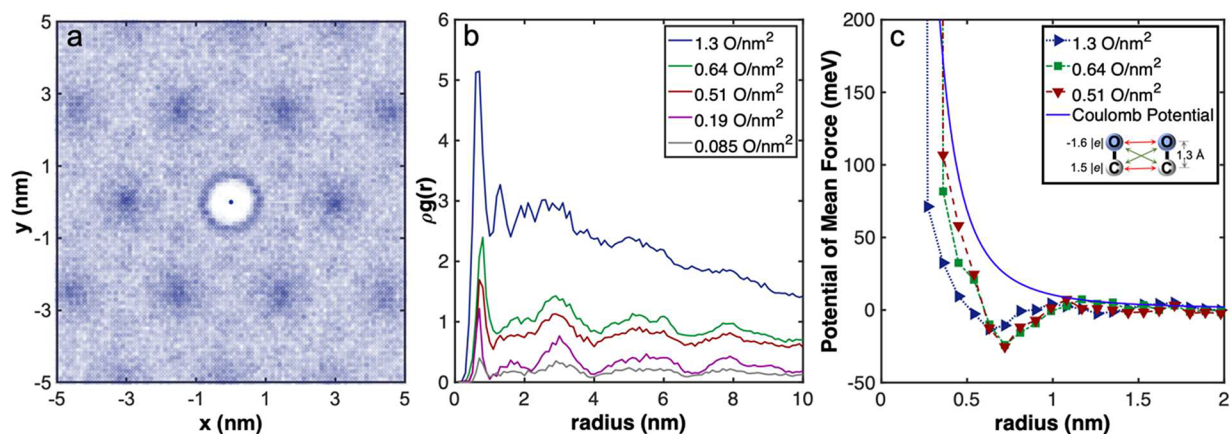

Figure 3. Oxygen−oxygen pair distribution functions. (a) Two-dimensional pair distribution function for an average oxygen coverage of 0.51 O/nm^2 on G/Ru(0001). Each point corresponds to a pair of O atoms found in STM topography. (b) One-dimensional pair distributions for O atoms on G/Ru(0001) with increasing coverage 0.085−1.3 O/nm^2. The most prominent peak corresponds to oxygen atoms in the same FCC (or HCP) binding region. (c) The potential of mean force between two oxygen functional groups is calculated from radial distributions, and a Coulombic potential is plotted from DFT values for the C−O bond length, partial charges, and the dielectric constant of graphene.[13,27]

surface coverage of 0.64 O/nm^2 (5 oxygen atoms per 12 × 11 moiré unit cell) an average 2.3 O atoms are bound in an individual HCP region and 2.7 O in each FCC region at 300 K. Surface diffusion is also enhanced with higher coverages allowing equilibrium distributions to be reached at shorter time scales.

Site specificity of atomic oxygen binding is coverage dependent. At lower coverages (Figure 2f,g), oxygen atoms are confined largely to the middle of the FCC and HCP regions. As more oxygen atoms bind to the surface, O atoms are less likely to be in the center of FCC or HCP regions (Figure 2h,i) due to packing configurations that form as more than one O atom occupies a region of the moiré unit cell. As coverage increases further, a larger portion of the moiré cell is occupied, but atop regions and sites bridging the FCC/HCP regions remain largely unoccupied (Figure 2j). These configurations are due to steric effects of oxygen atom packing on the surface while repulsive oxygen−oxygen potentials are avoided (Figure 3c). Atop regions devoid of oxygen even with increasing $O(^3P)$ exposures illustrate the ability of moiré

templating to tailor the location of adsorbed oxygen even outside the low coverage limit. Surface populations across the unit cell (Figure 2f−j) are used to calculate the adsorption energy of O(^{3}P) across the moiré interface (Figure 2k−o). These results emphasize higher adsorption energies at atop sites and the areas bridging FCC and HCP regions on the moiré lattice, which limit diffusion of O atoms between HCP and FCC sites.

Directed placement of oxygen adatoms on stable 2D materials through moiré-templated oxidation requires a detailed understanding of oxygen−oxygen interactions at the surface. The location of oxygen atoms on the G/Ru(0001) moiré pattern is influenced by repulsive oxygen−oxygen interactions. Oxygen atoms do not bind within ∼0.55 nm of one another on the G/Ru(0001) surface as illustrated in O−O pair distribution functions (Figure 3). This observation fits well with the prediction that nonreactive scattering of O(^{3}P) from graphene increases as preadsorbed oxygen atoms repulse incident atoms due to both coverage and changes in surface electronic structure.[7]

We quantify the occurrence of the O−O interactions using the potential of the mean force between adsorbed oxygen atoms. The potential of mean force, $w(r)$, is calculated from pair distribution functions for oxygen atoms, $g(r)$, using eq 2:

$$w(r) = -k_BT \ln(g(r)) \qquad (2)$$

The potential of the mean force for the three highest oxygen coverages is plotted in Figure 3c. The length scale of repulsive interactions between O atoms fits well with a Coulombic model of charge attractions (Figure 3c). The Coulombic potential in Figure 3c models the interactions between enolate (C−O) functional groups as a sum of pairwise potentials between oxygen atoms and oxygen bound carbon atoms and takes into account the partial charge of oxygen ($-1.6|e|$), the charge of carbon ($1.5|e|$), and the C−O bond length (1.3 Å) from previous DFT work[13] along with the dielectric constant for graphene ($6.9\varepsilon_0$).[27]

Repulsive interactions, quantified in Figure 3c as a potential of mean force between two oxygen adatoms, are seen to affect binding specificity on the moiré unit cell; avoided regions in the center of HCP and FCC regions arise from the excluded regions surrounding O atoms (Figure 2h,i). Nearest-neighbor oxygen atoms often bind ∼0.7 nm apart (Figure 3), and at higher coverage (1.3 O/nm^2, Figure 3b) a second-order peak (∼1.3 nm) appears in the O−O radial distribution function. Nanoscale periodicity of oxygen atoms illustrates how adsorbate interactions on discrete lattice sites can tune the distance between adatoms for the moiré-templated synthesis of 2D materials.

Coverage dependence of oxygen diffusion on single-crystalline surfaces has been shown previously on a wide variety of metallic, semiconducting, and other interfaces;[28−30] however, corrugation in the potential energy surface across the moiré pattern opens a new regime in measuring atomistic interfacial diffusivity. While G/Ru(0001) is a single crystalline system—its massive 25 × 25 graphene unit cell encompasses 1250 carbon atoms and offers a diverse range of binding geometries. The effects that neighboring oxygen atoms have on binding energies and diffusion barriers provide additional complexity to the system. Accurately modeling the diffusivity of atomic oxygen at higher oxygen coverages on the G/Ru(0001) interface will prove to be an interesting challenge as

oxygen diffusion from one site to another on the unit cell is not well described by one universal diffusion barrier.

Illustrating this, oxygen atoms were observed to diffuse in both FCC and HCP regions, with HCP bound oxygen atoms being more mobile on the surface. An example of STM oxygen diffusion is seen in Figure 4A,B. At 230 K and an average
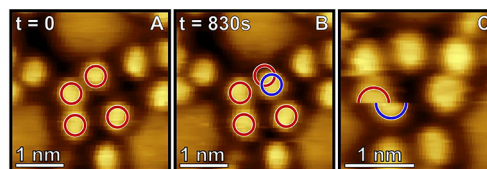

Figure 4. Visualization of O atoms hopping. (A) STM topography (−1.5 V, −250 pA) shows initial positions of four O atoms in an individual FCC moiré region (circled in red). (B) In the 830 s between two STM images, one O atom diffuses to a neighboring binding site (circled in blue). (C) An O atom hops between its initial (red) and final position (blue), while the STM is scanning over the O atom with sequential line scans. In this case, one atom is visualized as two semicircular protrusions in the same STM image indicating a jump in location. The 230 K surface had a global coverage of 1.0 O/nm^2.

coverage of 1.0 O/nm^2, chemisorbed O atoms hopped at a rate of $(2.6 \pm 0.2) \times 10^{-4}$ hops/s in HCP regions and $(1.3 \pm 0.1) \times 10^{-4}$ hops/s in FCC regions. As these measurements were made with a scanning probe, it is necessary to rule out tip-induced surface diffusion. In STM images collected, each individual oxygen atom is visualized over consecutive scanlines as our probe advances by subatomic increments per scanline. If the tip were to stimulate mobility of O atoms, then an O atom would be visualized in different locations in sequential scanlines within the same STM image as shown in Figure 4C.

Of 996 hopping events identified *via* STM (−1.5 V, −250 pA, 1.0 O/nm^2) at 230 K, only 13% of the O atoms hopped while within individual scanlines of an STM image (Figure 4C). During this experiment, each O atom is approximately 15 scanlines wide and occupies ∼6% of scanlines continuously collected between initial and final visualization. Therefore, a nonzero number of atoms thermally diffusing are expected to hop while the STM tip is actively scanning those atoms, as depicted in Figure 4C without STM tip-induced motion. At lower coverage (0.066 O/nm^2) and the same tunneling conditions (−1.5 V, −250 pA) at 300 K, ∼5% of O atoms which hopped did so between two successive scanlines. A lack of widespread visualization of individual O atoms hopping within the same STM image (as seen in Figure 4C) indicates that tip-induced motion is inconsequential.

At lower coverage (0.04 O/nm^2), surface diffusion persisted ($(5.0 \pm 0.3) \times 10^{-5}$ hops/s) at 300 K with tunneling conditions (200 mA, 100 pA) like those used in a previous study which demonstrated Arrhenius temperature dependence in hopping rates in a higher temperature regime (>400 K).[13] Building upon this previous work on oxygen diffusion, which investigated the low coverage regime at elevated temperatures, we identify coverage dependence and spatiotemporal correlations in surface diffusivity at temperatures ≤300 K.

STM topography enables monitoring of local surface morphologies to investigate how local configurations of adsorbates on the moiré lattice affect the diffusivity of oxygen adatoms. Adsorbate interactions increase the overall observed hopping rate at higher coverages through correlated diffusion
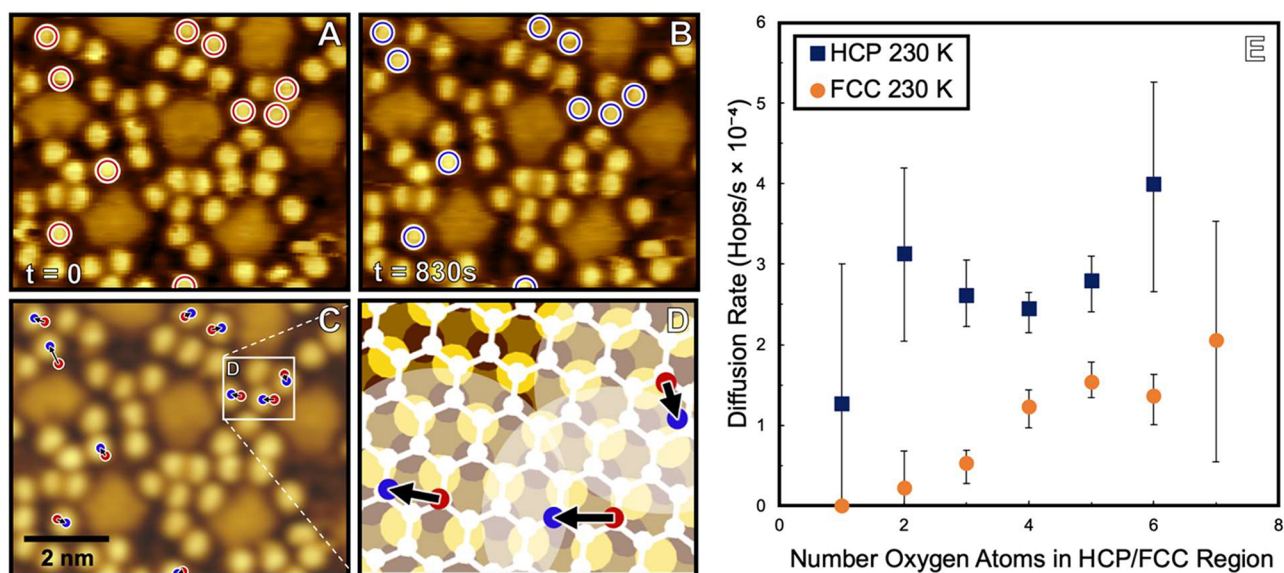
Figure 5. Atomistic visualization of oxygen diffusion on G/Ru(0001). (A, B) Sequential STM images (-1.5 V, -250 pA) of O atoms on G/Ru(0001) at 230 K. Atoms which hop to different binding sites between $t = 0$ and 830 s are circled in each image. (C) Arrows represent diffusion events from sequential images (A, B). (D) G/Ru(0001) is sketched to scale with the locations and diffusion vectors for the three atoms from (C). The excluded region around points from $t = 0$ are shaded white. (E) Diffusion of oxygen atoms on G/Ru(0001) was measured while monitoring the population of oxygen atoms in an individual FCC or HCP region. Average coverages were 3.8 O atoms/HCP region and 4.3 O atoms/FCC region, and 996 total hops were observed. 95% confidence intervals are plotted.

events, e.g., an O atom that diffuses into the excluded region (illustrated in Figure 3a) of a second O atom can propel the second O atom to hop as well.

An example of correlated diffusion is seen in Figure 5C,D where three oxygen atoms in proximity diffuse in the same 830 s interval. Note that each atom either is invading the excluded region of another adsorbate or is vacating an area into which another O atom hops in Figure 5d. The atomistic picture of diffusion in Figure 5d also supports the finding that oxygen binds as an enolate on the surface because oxygen atoms are "double hopping" on the graphene lattice, i.e., preferential binding sites occur at every other carbon atom.[13] While atomic oxygen typically binds in an epoxy geometry on free-standing graphene surfaces, enolate binding was predicted in a DFT study to be energetically favorable for epitaxial graphene on metal substrates due to the ability of underlying metal to compensate for instability introduced by atomic oxygen into graphene's π-conjugated system.[9] DFT studies additionally show charge transfer to oxygen adatoms is greater for enolate geometries, allowing for stronger Coulombic repulsions on the surface over larger length scales, like those seen in Figure 3c.[9,13]

STM scans reveal that local oxygen coverage affects surface diffusion. To illustrate this point, the average rate of diffusion increases from $(3.3 \pm 0.8) \times 10^{-4}$ to $(5.7 \pm 0.5) \times 10^{-4}$ hops/s when comparing HCP regions occupied by one oxygen versus HCP regions with two oxygen atoms at 300 K and a global coverage of 0.55 O/nm^2. Assuming that the preexponential for Arrhenius diffusion is the same for O atoms in both singly and doubly occupied HCP regions, this increase in rate points to a 0.014 eV reduction in the effective barrier to diffusion. Tracking local environment in this way, the rate of diffusion for HCP/FCC regions with increasing number of oxygen atoms is presented in Figure 5E. As more O atoms occupy the same FCC region, the diffusion rate trends upward. The effective barrier to diffusion decreases by 0.05 eV for O

atoms diffusing in a local FCC region when the occupancy is raised from two to seven oxygen atoms (Figure 5E) assuming Arrhenius diffusion with a constant preexponential. The local environment has varying effects on surface diffusion. While additional O atoms can facilitate diffusion by lowering the barrier to diffusion and through *correlated diffusion events* like those seen in Figure 5D, oxygen atoms on the surface occupy binding sites and can block potential hopping events as well. These competing effects lead to a nonmonotonic trend in diffusion rate as a function of local surface coverage as seen for HCP bound O atoms in Figure 5D.

We have shown that the diffusion rate of oxygen atoms on the moiré pattern of G/Ru(0001) is dependent upon local oxygen coverage. Looking at the local environment, we next gauge how correlated oxygen diffusion occurs on the G/Ru(0001) surface. As an example, consider three oxygen atoms in the same FCC region. It is possible for 0, 1, 2, or 3 oxygen atoms to hop to a different binding site between two successive STM images. At 300 K, the probability exactly 0, 1, 2, or 3 O atoms hop in a 940 s interval was measured to be 50 ± 7, 24 ± 6, 18 ± 5, and 8 ± 4%, respectively, for a triply occupied FCC region. To gauge correlation in oxygen hopping events, we compare these probabilities to a simple binomial model eq 3 for random hopping:

$$P(x) = \frac{p^x (1-p)^{n-x} n!}{x!(n-x)!} \tag{3}$$

This model accounts for the probability that any O atom hops in a 940 s interval ($p = 28$% for 3 O in an FCC region), how many O atoms are in that region ($n = 3$), and the number of O atoms that hop in 940 s ($x = 0, 1, 2,$ or 3). A binomial model for totally random hopping thus predicts the probability exactly 0, 1, 2, or 3 O atoms hop between two STM images to be 37, 44, 17, and 2%, respectively. The largest difference between experiment and the predicted values is for the situation in which exactly one of the three O atoms hops. This is a result of

correlation in O atom diffusion on the surface: surrounding O atoms either hopping in unison or blocking potential diffusion sites. The probability that exactly one O atom hops (and does not cause a subsequent hopping event) in a local region thus makes a useful metric for correlation in surface diffusion as shown in Figure 6.
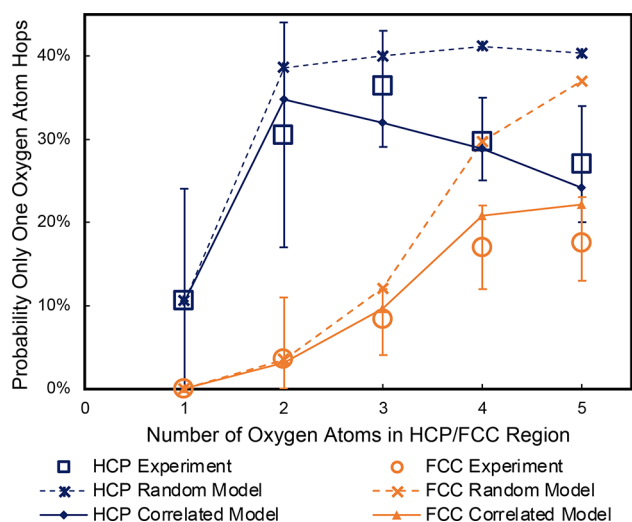

Figure 6. Correlated oxygen diffusion is dependent on local coverage. Diffusion of O on G/Ru(0001) was tracked at 230 K. The probability of observing exactly one oxygen atom hop in a local region after 830 s is plotted with 95% confidence intervals as a function of the number of oxygen atoms in that region. A simple binomial model in which hopping events are uncorrelated was generated by using the diffusion rates for each occupancy level reported in Figure 5e, and the likelihood that only one O atom would hop in each region after 830 s is plotted with dashed lines connecting the randomly predicted points to guide the eye. A correlated model in which O atoms have a 10% likelihood of hopping when another O atom hops more closely aligns with the experimental data, and lines are plotted to guide the eye.

Tracking the likelihood of only one oxygen atom hopping in singly through quintuply occupied HCP/FCC moiré regions demonstrates a simple random model with no correlation in the hopping of oxygen atoms performs worse with increasing coverage in FCC/HCP regions. Single-hopping events are increasingly underrepresented experimentally in comparison to a totally random model with increasing coverage. Conversely, multiple O atoms hopping in the same period are over-represented in the diffusion data collected in comparison to random diffusion. This indicates coordinated diffusion events like those seen in Figure 5d are not random occurrences but in fact systemic and influence the globally measured diffusion rates, illustrating the rich detail atomic resolution microscopy lends to understanding surface dynamics.

A correlated diffusion model can be generated by assuming that O atoms in a local region have a probability (b) of being induced into motion by a neighboring O atom hopping. The probability (C) that exactly one atom hops in a local region using this model for correlated diffusion is given in eq 4:

$$C = P(1)(1 - b(n - 1)) \qquad (4)$$

This correlated model is plotted in Figure 6 with $b = 10\%$, meaning that O atoms have a 10% chance of being stimulated to hop by a neighboring O atom hopping. An O atom occupies 10% of an individual HCP or FCC region's surface area when

accounting for a minimum 0.55 nm separation between adsorbates seen in pair distribution functions (Figure 3). Agreement of this model with experimental data, *specifically when b = 10%*, indicates that correlated diffusion is dependent on the length scale of repulsive potentials on the surface. That is, when O atoms hop into the excluded region of another adatom, that adatom is forced to hop as well.

Increasing oxygen coverage in this study demonstrates markedly different diffusion behaviors in both overall diffusivity and the correlated motion of oxygen on the surface. Understanding how surface dynamics change at an atomistic level as systems become more complex lends valuable insight for understanding the fundamental on-surface dynamics that determine rate constants, material properties, and the site specificity and stability of adatom placement on two-dimensional materials.

Moiré-templated oxidation of graphene was accomplished *via* reactive scattering of O(^{3}P) onto G/Ru(0001). Careful monitoring of local surface morphologies revealed that neighboring oxygen atoms both increased surface diffusivity and led to correlated hopping on the surface. The site specificity of oxygen binding was found to be coverage dependent with repulsive forces between oxygen atoms affecting the partitioning of binding even at coverages far below saturation. Results demonstrate how *in situ* microscopy provides incisive insight into on-surface dynamics when paired with supersonic molecular beams, which provide tight control of the incident angle and kinetic energy of impinging O(^{3}P), allowing for the investigation of new regimes of non-equilibrium interfacial gas−surface oxidation dynamics. On-going studies pairing molecular beam exposures and STM visualization promise a route to the intentional placement of oxygen atoms at specific moiré sites as a function of incident beam kinetic conditions. Results further illustrate the creation of self-assembled ordered arrays of atomic oxygen through moiré templating promising facile top-down synthesis of graphene-based quantum materials and other 2D functionalized materials.

Experimental Methods. Atomic visualization of the G/Ru(0001) surface was accomplished with a UHV instrument which combines an *in situ* STM in line with a triply differentially pumped molecular beam described previously in detail.[31−33] The scanning probe microscope (SPM) chamber ($<1 \times 10^{-11}$ Torr base pressure) contains a custom-built variable temperature Pan SPM.[31,32] STM images were taken using cut and pulled Pt$_{0.8}$Ir$_{0.2}$ tips.

Atomic oxygen was generated using an RF plasma source primarily producing ground-state atomic oxygen, O(^{3}P).[34] Neat O_2 was ignited and expanded through a water-cooled glass nozzle, and isenthalpic expansion produces O(^{3}P) with an average 0.07 eV translational kinetic energy. The backing pressure (10 Torr) and RF power (170 W) were tuned to maximize the O(^{3}P) flux, $\sim 7 \times 10^{10}$ O atoms cm^{-2} s^{-1}.

The Ru(0001) crystal (Surface Preparation Laboratory, 99.99% purity) used in this study was cleaned in the characterization/preparation chamber ($<1 \times 10^{-10}$ Torr base pressure) by sputtering 0.5 eV Ar$^+$ ions resulting in a current of 0.1−0.5 μA cm^{-2} on the sample and annealing by electron beam bombardment to 1500 K (10 s) between sputter cycles; crystal quality was assessed using LEED, AES, and STM.[31] A pristine graphene monolayer was created by annealing the Ru(0001) single crystal at 900 K with an overpressure of C_2H_4

$(5 \times 10^{-6}$ Torr$)$ for 5 min followed by annealing the crystal to 1200 K for 1 min and slowly cooling over a 10 min period.

■ AUTHOR INFORMATION

Corresponding Author

Steven J. Sibener − *The James Franck Institute and Department of Chemistry, The University of Chicago, Chicago, Illinois 60637, United States;* orcid.org/0000-0002-5298-5484; Email: s-sibener@uchicago.edu

Author

Joshua Wagner − *The James Franck Institute and Department of Chemistry, The University of Chicago, Chicago, Illinois 60637, United States*

Complete contact information is available at:
https://pubs.acs.org/10.1021/acs.jpclett.4c00274

Notes

The authors declare no competing financial interest.

■ ACKNOWLEDGMENTS

■ REFERENCES

(1) Liu, X.; Hersam, M. C. 2D Materials for Quantum Information Science. *Nat. Rev. Mater.* **2019**, *4* (10), 669−684.

(2) Lemme, M. C.; Akinwande, D.; Huyghebaert, C.; Stampfer, C. 2D Materials for Future Heterogeneous Electronics. *Nat. Commun.* **2022**, *13* (1), 1392.

(3) Tierney, H. L.; Murphy, C. J.; Jewell, A. D.; Baber, A. E.; Iski, E. V.; Khodaverdian, H. Y.; McGuire, A. F.; Klebanov, N.; Sykes, E. C. H. Experimental Demonstration of a Single-Molecule Electric Motor. *Nat. Nanotechnol.* **2011**, *6* (10), 625−629.

(4) Johns, J. E.; Alaboson, J. M. P.; Patwardhan, S.; Ryder, C. R.; Schatz, G. C.; Hersam, M. C. Metal Oxide Nanoparticle Growth on Graphene via Chemical Activation with Atomic Oxygen. *J. Am. Chem. Soc.* **2013**, *135* (48), 18121−18125.

(5) Cao, Y.; Fatemi, V.; Fang, S.; Watanabe, K.; Taniguchi, T.; Kaxiras, E.; Jarillo-Herrero, P. Unconventional Superconductivity in Magic-Angle Graphene Superlattices. *Nature* **2018**, *556* (7699), 43−50.

(6) Kögl, M.; Soubelet, P.; Brotons-Gisbert, M.; Stier, A. V.; Gerardot, B. D.; Finley, J. J. Moiré Straintronics: A Universal Platform for Reconfigurable Quantum Materials. *npj 2D Mater. Appl.* **2023**, *7* (1), 32.

(7) Jayee, B.; Nieman, R.; Minton, T. K.; Hase, W. L.; Guo, H. Direct Dynamics Simulations of Hyperthermal O(^{3}P) Collisions with Pristine, Defected, Oxygenated, and Nitridated Graphene Surfaces. *J. Phys. Chem. C* **2021**, *125* (18), 9795−9808.

(8) Marchini, S.; Günther, S.; Wintterlin, J. Scanning Tunneling Microscopy of Graphene on Ru(0001). *Phys. Rev. B* **2007**, *76* (7), No. 075429.

(9) Jung, J.; Lim, H.; Oh, J.; Kim, Y. Functionalization of Graphene Grown on Metal Substrate with Atomic Oxygen: Enolate vs Epoxide. *J. Am. Chem. Soc.* **2014**, *136* (24), 8528−8531.

(10) Feng, X.; Kwon, S.; Park, J. Y.; Salmeron, M. Superlubric Sliding of Graphene Nanoflakes on Graphene. *ACS Nano* **2013**, *7* (2), 1718−1724.

(11) Lu, J.; Yeo, P. S. E.; Gan, C. K.; Wu, P.; Loh, K. P. Transforming C60 Molecules into Graphene Quantum Dots. *Nat. Nanotechnol.* **2011**, *6* (4), 247−252.

(12) Martoccia, D.; Willmott, P. R.; Brugger, T.; Björck, M.; Günther, S.; Schlepütz, C. M.; Cervellino, A.; Pauli, S. A.; Patterson, B. D.; Marchini, S.; Wintterlin, J.; Moritz, W.; Greber, T. Graphene on Ru(0001): A 25 × 25 Supercell. *Phys. Rev. Lett.* **2008**, *101* (12), No. 126102.

(13) Novotny, Z.; Nguyen, M.-T.; Netzer, F. P.; Glezakou, V.-A.; Rousseau, R.; Dohnálek, Z. Formation of Supported Graphene Oxide: Evidence for Enolate Species. *J. Am. Chem. Soc.* **2018**, *140* (15), 5102−5109.

(14) Wang, B.; Bocquet, M.-L.; Marchini, S.; Günther, S.; Wintterlin, J. Chemical Origin of a Graphene Moiré Overlayer on Ru(0001). *Phys. Chem. Chem. Phys.* **2008**, *10* (24), 3530.

(15) Vinogradov, N. A.; Schulte, K.; Ng, M. L.; Mikkelsen, A.; Lundgren, E.; Mårtensson, N.; Preobrajenski, A. B. Impact of Atomic Oxygen on the Structure of Graphene Formed on Ir(111) and Pt(111). *J. Phys. Chem. C* **2011**, *115* (19), 9568−9577.

(16) Hossain, Md. Z.; Johns, J. E.; Bevan, K. H.; Karmel, H. J.; Liang, Y. T.; Yoshimoto, S.; Mukai, K.; Koitaya, T.; Yoshinobu, J.; Kawai, M.; Lear, A. M.; Kesmodel, L. L.; Tait, S. L.; Hersam, M. C. Chemically Homogeneous and Thermally Reversible Oxidation of Epitaxial Graphene. *Nat. Chem.* **2012**, *4* (4), 305−309.

(17) Zhang, Z.; Yin, J.; Liu, X.; Li, J.; Zhang, J.; Guo, W. Substrate-Sensitive Graphene Oxidation. *J. Phys. Chem. Lett.* **2016**, *7* (5), 867−873.

(18) Li, G.; Zhou, H. T.; Pan, L. D.; Zhang, Y.; Mao, J. H.; Zou, Q.; Guo, H. M.; Wang, Y. L.; Du, S. X.; Gao, H.-J. Self-Assembly of C60 Monolayer on Epitaxially Grown, Nanostructured Graphene on Ru(0001) Surface. *Appl. Phys. Lett.* **2012**, *100* (1), No. 013304.

(19) Zhang, H. G.; Sun, J. T.; Low, T.; Zhang, L. Z.; Pan, Y.; Liu, Q.; Mao, J. H.; Zhou, H. T.; Guo, H. M.; Du, S. X.; Guinea, F.; Gao, H.-J. Assembly of Iron Phthalocyanine and Pentacene Molecules on a Graphene Monolayer Grown on Ru(0001). *Phys. Rev. B* **2011**, *84* (24), No. 245436.

(20) Zhou, Z.; Gao, F.; Goodman, D. W. Deposition of Metal Clusters on Single-Layer Graphene/Ru(0001): Factors That Govern Cluster Growth. *Surf. Sci.* **2010**, *604* (13−14), L31−L38.

(21) Donner, K.; Jakob, P. Structural Properties and Site Specific Interactions of Pt with the Graphene/Ru(0001) Moiré Overlayer. *J. Chem. Phys.* **2009**, *131* (16), No. 164701.

(22) Nieman, R.; Sands, M.; Wang, Y.; Minton, T. K.; Mussoni, E. E.; Engerer, J.; Guo, H. Informing Air−Carbon Ablation Modeling with Theoretical Calculations of Atomic Oxygen and Nitrogen Interacting with Carbon Surfaces. *Phys. Chem. Chem. Phys.* **2023**, *25* (22), 15479−15489.

(23) Zhao, Z.; Wang, Y.; Yang, X.; Quan, J.; Krüger, B. C.; Stoicescu, P.; Nieman, R.; Auerbach, D. J.; Wodtke, A. M.; Guo, H.; Park, G. B. Spin-Dependent Reactivity and Spin-Flipping Dynamics in Oxygen Atom Scattering from Graphite. *Nat. Chem.* **2023**, *15*, 1006−1011.

(24) Migliorini, D.; Chadwick, H.; Nattino, F.; Gutiérrez-González, A.; Dombrowski, E.; High, E. A.; Guo, H.; Utz, A. L.; Jackson, B.; Beck, R. D.; Kroes, G.-J. Surface Reaction Barriometry: Methane Dissociation on Flat and Stepped Transition-Metal Surfaces. *J. Phys. Chem. Lett.* **2017**, *8* (17), 4177−4182.

(25) Badan, C.; Farber, R. G.; Heyrich, Y.; Koper, M. T. M.; Killelea, D. R.; Juurlink, L. B. F. Step-Type Selective Oxidation of Platinum Surfaces. *J. Phys. Chem. C* **2016**, *120* (40), 22927−22935.

(26) Swenson, H.; Stadie, N. P. Langmuir's Theory of Adsorption: A Centennial Review. *Langmuir* **2019**, *35* (16), 5409−5426.

(27) Fang, J.; Vandenberghe, W. G.; Fischetti, M. V. Microscopic Dielectric Permittivities of Graphene Nanoribbons and Graphene. *Phys. Rev. B* **2016**, *94* (4), 045318.

(28) Inderwildi, O. R.; Lebiedz, D.; Deutschmann, O.; Warnatz, J. Coverage Dependence of Oxygen Decomposition and Surface

Diffusion on Rhodium (111): A DFT Study. *J. Chem. Phys.* **2005**, *122* (3), No. 034710.

(29) Chen, J.-R.; Gomer, R. Mobility of Oxygen on the (110) Plane of Tungsten. *Surf. Sci.* **1979**, *79* (2), 413−444.

(30) Binnig, G.; Fuchs, H.; Stoll, E. Surface Diffusion of Oxygen Atoms Individually Observed by STM. *Surface Science Letters* **1986**, *169* (2−3), L295−L300.

(31) Wagner, J.; Grabnic, T.; Sibener, S. J. STM Visualization of N_2 Dissociative Chemisorption on Ru(0001) at High Impinging Kinetic Energies. *J. Phys. Chem. C* **2022**, *126* (43), 18333−18342.

(32) Edel, R.; Grabnic, T.; Wiggins, B.; Sibener, S. J. Atomically-Resolved Oxidative Erosion and Ablation of Basal Plane HOPG Graphite Using Supersonic Beams of O_2 with Scanning Tunneling Microscopy Visualization. *J. Phys. Chem. C* **2018**, *122* (26), 14706−14713.

(33) Wiggins, B.; Avila-Bront, L. G.; Edel, R.; Sibener, S. J. Temporally and Spatially Resolved Oxidation of Si(111)-(7 × 7) Using Kinetic Energy Controlled Supersonic Beams in Combination with Scanning Tunneling Microscopy. *J. Phys. Chem. C* **2016**, *120* (15), 8191−8197.

(34) Sibener, S. J.; Buss, R. J.; Ng, C. Y.; Lee, Y. T. Development of a Supersonic $O(^3P_J)$, $O(^1D_2)$ Atomic Oxygen Nozzle Beam Source. *Rev. Sci. Instrum.* **1980**, *51* (2), 167−182.